Mon. Not. R. Astron. Soc. **000**, 1–6 (2015) Printed 20 April 2015 (MN LATEX style file v2.2)

# Scintillation Distance Measurements

Siqi Liu[1,3⋆], Ue-Li Pen[1,2]†, J-P Macquart[4]‡, Walter Brisken[5]§, Adam Deller[6]¶
[1] *Canadian Institute for Theoretical Astrophysics, University of Toronto, M5S 3H8 Ontario, Canada*
[2] *Canadian Institute for Advanced Research, Program in Cosmology and Gravitation*
[3] *Department of Astronomy and Astrophysics, University of Toronto, M5S 3H4, Ontario, Canada*
[4] *ICRAR-Curtin University of Technology, Department of Imaging and Applied Physics, GPO Box U1978, Perth, Western Australia 6102, USA*
[5] *National Radio Astronomy Observatory, P.O. Box O, Socorro, NM 87801, USA*
[6] *ASTRON, the Netherlands Institute for Radio Astronomy, Postbus 2, 7990 AA, Dwingeloo, The Netherlands*

20 April 2015

**ABSTRACT**
We show how interstellar scintillations, combined with VLBI measurements, can be used to measure distances. We apply the technique to archival data on PSR B0834+06, concluding that for this example the plasma lenses can be precisely modelled using the Pen and Levin (2014) inclined sheet model, resulting in two distinct lens planes. This data strongly favours the reconnection sheet model over turbulence as the primary source of pulsar scattering. A global conformal distance degeneracy exists which allows a rescaling of the absolute distance scale. This degeneracy is broken if the pulsar resides in a binary system, which is the case for most precision timing targets.

**Key words:** Pulsar

## 1 INTRODUCTION

Pulsars have long provided a rich source of astrophysical information due to their compact emission and predictable timing. One of the weakest measurements for most pulsars is their direct geometric distance. For some pulsars, timing parallax or VLBI parallax has resulted in direct distance determinations. For most pulsars, the distance is a major uncertainty for precision timing interpretations, including mass, moment of inertia, and gravitational wave direction (Boyle & Pen 2012).

Direct VLBI observation of PSR B0834+06 shows multiple images lensed by the interstellar plasma. Combining the angular positions and scintillation delays, the authors published the derived effective distance (Brisken et al. 2010) of approximately $1168 \pm 23$ pc for apexes whose time delays range from 0.1 ms to 0.4 ms, and $1121 \pm 59$ pc for 1 ms apexes. This represents a precise measurement compared to all other attempts to derive distances to this pulsar. This effective distance is a combination of pulsar-screen and earth-screen distances, and does not allow a separate determination of the individual distances. A binary pulsar system would in principle allow a breaking of this degeneracy (Pen & Levin 2014). One potential limitation is the precision to which the lensing model can be understood. In this paper, we demonstrate that the lensing screen consists of nearly parallel linear refractive structures, in two screens. The precise model confirms the one dimensional nature, and thus the small number of parameters that need to be measured to quantify the lensing screen.

⋆ E-mail: sqliu@cita.utoronto.ca
† E-mail: pen@cita.utoronto.ca
‡ E-mail:J.Macquart@curtin.edu.au
§ Email:wbrisken@aoc.nrao.edu
¶ E-mail:deller@astron.nl

## 2 LENSING

### 2.1 B0834+06

Our analysis is based on the reduced apex catalog from Brisken et al. (2010). Information from each identified apex includes delay $\tau$, delay rate (differential frequency $f_D$), RA and dec. Data of each apex are collected from four 8 MHz wide sub-bands centering 314.5 MHz, 322.5 MHz, 328.5 MHz and 334.5 MHz. We mapped a total of 9 apexes from the 0.4 ms group, and 5 from the 1 ms group. This results in an estimation for the average value and standard deviation among four sub-bands, we list the average value in $f = 322.5$ MHz in Table 2.4.2. The time is calculated with $2\tau f/f_D$, equivalent to pulsar moving at 640 pc plane from the original position to the lensed image position with the calculated proper motion of the pulsar.

The way we use to calculate the error of time delay $\tau$ and differential frequency $f_D$ is by the following equation:

$$\sigma = \sqrt{\sum^{i} \frac{1}{{\sigma_i}^2}},$$

which is also how we calcualte the population error of RA and dec, marked with circles in Figure 2. The way we use to calculate the sample error of RA and dec, is defined by following equation:

$$\sigma = \sqrt{\frac{\sum_{i=1}^{n}(x_i - \mu)^2}{n(n-1)}},$$

and they are marked with errorbars in Figure 2.

How distance of the pulsar is related to the time delay and how velocity is related to the differential frequency are defined by the following equations:

$$\tau = \frac{D_{\rm e}\theta^2}{2c},$$
$$f_D = f \cdot \frac{\delta\tau}{dt},$$

where $D_{\rm e}$ is the effective distance, equivalent to the lens placing at the middle point of the pulsar: $D_{\rm e} = D_p D_s/(D_p - D_s)$.

A least square effective distance results in $D_e^1 = 1017.1 \pm 2.8$ for the 0.4 ms apexes on lens 1and $D_e^2 = 1243 \pm 64$ for the 1 ms apexes on lens 2. This seems to indicate that the lens 1 is closer to the pulsar. The error bars are large enough to allow them to be at the same distance, or perhaps a reverse distance ordering. In this paper, we present two analyses for comparison: equidistant, and at the best fit distances. In the first case, no direct distance measurement is possible, but it nevertheless illustrates a robust interpretation of the data.

### 2.2 Lens Solution

In order to interpret the data, we adopt the lensing model of Pen & Levin (2014). In the absence of a lens model, the fringe rate, delay and angular position cannot be uniquely related. In this model, the lensing is due to projected fold caustics of a thin sheet closely aligned to the line of sight.

Furthermore, if we know the distance of the pulsar is 640 pc by parallax, the screen, named lens 1, where 0.4 ms scintillation points are refracted, $D_s^1$ is equal to 392.8 pc. We know the position of the axis angle, with an $\alpha$ $-25.2$ degree away from the north axis (if the east direction is set to be the positive direction), and the positions of the 0.4 ms group are calculated:

$$\mathrm{RA} = -\theta \cdot \sin\alpha,$$
$$\mathrm{dec} = -\theta \cdot \cos\alpha.$$

They are marked out with the scatter points on the left side of Figure 2. For 1 ms apexes, the distance of lens 2 $D_s^2$, is equal to 422.5 pc. Thus, the degeneracy of the distance of the screen is broken.

We calculate the positions of the 1 ms apexes in following steps. First, matching the $\theta$-$\tau$ relation, which is plotted in Figure 1, we calculate the $\theta$ from observation $\tau$. Note that we define the velocity that is in the direction of the pulsar. Second, we consider the point with the largest $\theta$ among this 1 ms group, named 5, share the same $\theta_\parallel$ with the point with the largest $\theta$ among the 0.4 ms group, named 6. $\theta_\perp$ is calculated by $\theta_\perp = \sqrt{\theta^2 - \theta_\parallel^2}$. Then, by using a rotation matrix defined by $\alpha$, the position of point 5 is determined.

Third, to determine the position of the rest points $1-4$, we need to know the velocity of the pulsar, and then to fit the RA and dec to get the same differential frequency with the observation. To know the velocity of the pulsar, we calculated the velocity component in two directions: $v_\parallel$ according to the differential frequency of point 6 in 0.4 ms group; and $v_{\rm A5}$ (in the direction pointing from point 5 to A) according to the differential frequency of point 5. More specifically, to solve two equations:

$$\tau(t = 0\mathrm{s}) - \tau(t = 6500\mathrm{s}, v_\parallel) = f_{D6}/f \cdot \mathrm{dt},$$
$$\tau(t = 0\mathrm{s}) - \tau(t = 6500\mathrm{s}, v_{A5}) = f_{D5}/f \cdot \mathrm{dt},$$

where $f = 322.5$ MHz. Then we know the $v_\perp$ component by $v_{A5}$, and furthermore, the total velocity of the pulsar $v_{tot}$ and its angle to the north axis $\delta$, note that the east direction is the positive direction.

Fourth, we fit the position of the rest four points, with known proper motion of the pulsar. For example, point 4:

$$\tau(t = 0\mathrm{s}) - \tau(t = 6500\mathrm{s}, v_{A4}) = f_{D4}/f \cdot \mathrm{dt},$$
$$v_{\rm tot} \cdot \cos[\mathrm{atan}(\mathrm{RA}, \mathrm{dec}) + \pi/2 - \delta] = v_{A4},$$
$$\theta_4^2 = \mathrm{RA}^2 + \mathrm{dec}^2$$

We fit a line to this five calculated points, to describe these the positions of these 5 points.

That is one lens model fitting. Knowing time delay $\tau$, we can get the distance of the screen; knowing the position of point 5 and the differential frequency $f_D$, we can get the velocity of the pulsar; knowing the velocity and observation diffferential frequency, we can get the position of points $1-4$.

### 2.3 Discussion of one lens model

The 0.4 ms group lens solution appears consistent with the premise of the inclined sheet lensing model (Pen & Levin 2014).

For 1 ms group, lens 2 only images a subset of the lens 1 images. This could happen if lens 1 screen is just under the critical inclination angle, such that only $3-\sigma$ waves lead to a fold caustic. If the lens 2 was at a critical angle, the chance of encountering a somewhat less inclined system is of order unity. More surprising is the absence of a single refraction image of the pulsar, which is expected at position J. This could happen if the maximum refraction angle is just below critical, such that only rays on the appropriately aligned double refraction can form images. This scenario predicts that at frequencies just below 300 MHz, or a few weeks earlier in time, the pulsar should be seen at position J. We made a plot of the refraction angle $\beta$ in the direction that is transverse to the first lens plane in Figure 5. From our calculation, it takes 22 days for the puslar to move from point 1 on lens 1 to J, and it takes 44 days for the pulsar to move from point 5 on lens 1 to J. The data spans about 10% in frequency, making it unlikely that single lens image J would not be seen due to the larger required refraction angle. Instead, we speculate that the fold caustic could have formed near double lens image 1, and thus only intersections with the closer lens plane caustic south of image 1 are double lensed.

### 2.4 Double lens model

#### *2.4.1 Solving the double lens model*

We name the position of the pulsar point A, position of the lensed image on lens 2 point H, position of the lensed image on lens 1 point B, position of the observer O, pedal from the pulsar to line HE J, the pedal from point H to line BD F, and the pedal from point B to line HE G, for easier discussion. Because points $1-4$ share the approximately same time delay with the 5 points, the lens where the image formed should be at the same distance away from us. The only reasonable position of screen (line HE) that fits all these five points, marked with a solid line in Figure 2. However, in this senario, the screens cross each other, which means HE crosses with each other. That is unrealistic for the structure of the interstellar medium.

Therefore, we consider another model candidate: the double lens model. Respective calculation shows that the light is first refracted by the lens 2 and then refracted by lens 1.

The first step is to calculate the position of J. We make an estimate of the distance of J by the 1 ms $\theta-\tau$ relation, and then we calculated the position of J by matching the time delay of point 2 and point 5. The result shows that lens 2 is 425 pc away from us. And its position is marked in Figure 2. Because J is the pedal to lens 2, we made a line that is perpendicular to AJ, the solid line in Figure 2.

The second step is to find the matched pairs of those two lenses. By try and error, we found that the 5 points in 0.4 ms group that have the largest $\theta$ should be the candidates where lens 1 lie. These five matched lines are marked with dot dash lines in Figure 2 and their values are listed in the first two columns in Table 2.4.2. They are the located at a distance 392.8 pc away from us. Here we define three distances:

$$d_1 = 640 \text{ pc} - 425.0 \text{ pc} = 215.0 \text{ pc},$$
$$d_2 = 425 \text{ pc} - 392.8 \text{ pc} = 32.2 \text{ pc},$$
$$d_3 = 392.8 \text{ pc} - 0 \text{ pc} = 392.8 \text{ pc},$$

where $d_1$ is for the distance from the pulsar to lens 2, $d_2$ is for the distance from lens 2 to lens 1, and $d_3$ is for the distance from lens 1 to the observer.

Figure 3 and Figure 4 are examples of how light are being refracted on the first lens plane and the second lens plane. We specifically chose the point with $\theta_\parallel$ equal to $-17.44$ mas on lens 1 for instance. We solve the solutions in double lens model by following equations:

$$\frac{\text{JH}}{d_1} = \frac{\text{HG}}{d_2},$$
$$\frac{\text{FB}}{d_2} = \frac{\text{BD}}{d_3}.$$

The solved positions are plotted in Figure 2, and respective time delays and differential frequencies are listed in Table 2.4.2. For the error of time delay and differential frequency, we just use the following equation:

$$\sigma = \sqrt{\sigma_1^2 + \sigma_2^2},$$

where $\sigma_1$ represents the error from lens 1, and $\sigma_2$ represents the error from lens 2.

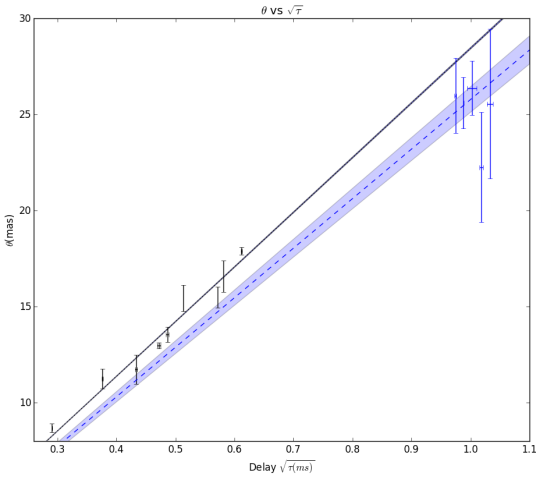


**Figure 1.** $\theta$ vs $\sqrt{\tau}$. The solid line is the fitted line of the 0.4ms positions, where $k = 28.51$ with an error region of $\sigma_k = 0.04$. The dashed lines are the fitted lines of the 1ms position, where $k = 25.78$ with an error region of $\sigma_k = 0.66$.

#### *2.4.2 Comparing calculated result in double lens model and observation data*

Comparing $\tau$, we time delay for these five points, and list the results in Table 2.4.2. For point 2 and 5, they fit perfectly because we use these two points to calculate the position of J; for the rest three points, all of the calculated results are still within $3-\sigma$ region of the observation time delays.

To compare differential frequency $f_D$, we need to calculate the velocity of the pulsar and the velocity of the lens. We consider lens 1 to be relative static, both the velocity of the pulsar and the velocity of lens 2 mentioned later are the relative velocities to lens 1. To calculate the velocity of the pulsar, we need two components, the $v_\parallel$ in the direction of the axis that $\alpha$ defined, and $v_\perp$ that is transverse to that axis. For $v_\parallel$, we still use the velocity that is calculated in 0.4 ms group in one lens model, that is 180.3 km/s. For the velocity of lens 2, because it is a line, and we do not consider radial velocity, so it could only be in the direction of AJ. However, by calculation, the angle of DAH is 98 degrees by calculation, that means $v_\perp$ and $v_{\text{lens2}}$ are degenerate. In the following discussion, we only consider $v_\perp$ and consider the $v_{\text{lens2}}$ to be static.

To calculate $v_\perp$, we choose the point 2, which has the smallest errorbar of differential frequency. In a time period of 6500 s, we solved that the $v_\perp$ should be 7.3 km/s, in the direction pointing from B to D, to make the calculated $f_D2$ match the observation $f_D$. Thus the $v_{tot}$ is solved to be 192.6 km/s, with an angle $\delta$ 4.59 degree west of north, which is marked on the top of the star in Figure 2.

## 3 POSSIBLE IMPROVEMENTS

We discuss several strategies which can improve on the solution accuracy. The single biggest improvement would be to monitor over a week, when the pulsar crosses each individual lens, including both lensing systems.

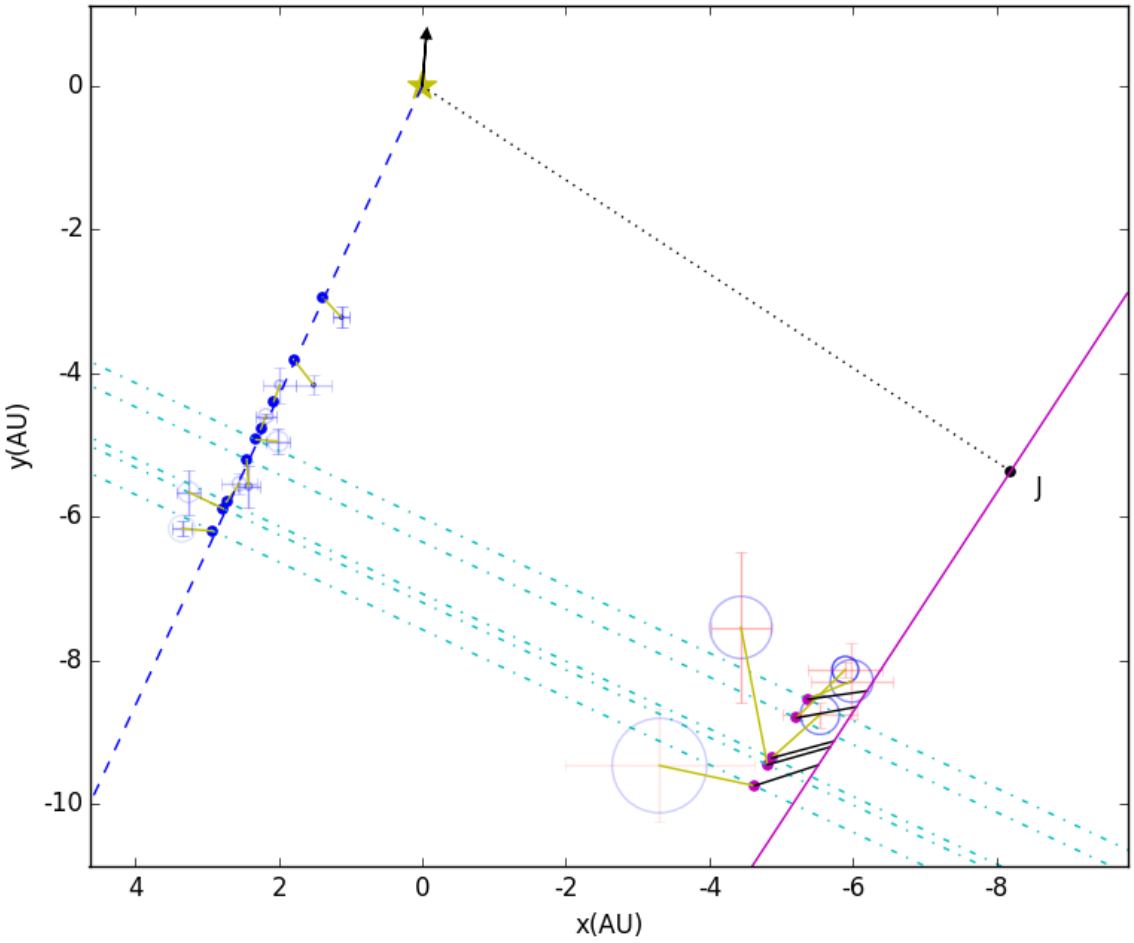


**Figure 2.** Observation data and calculated positions of 1 ms and 0.4 ms data of double lens model. In both apexes groups, the position of the screen locate at 392.8 pc and 425.0 pc. Scatter points on the left side are the points that fitted from the $f_D$ and $\tau$ of from the 0.4 ms apexes observation. Dash line is the fitted line of 0.4 ms apexes positions, with a angle $\alpha$ 25.2 degree west of north. The points lie on the left side with errorbars, are the observation points together with their sample errors; while the circles are plotted with population errors. Short solid lines between them are the matched positions of the observation positions and the calculated positions. The points on the right side are the points that fitted from the $f_D$ and $\tau$ of the 1 ms apexes. Solid line is the fitted line of these positions. Those points with errorbars nearby are the observation points together with their sample errors, while the circles are plotted with population errors. The dotted line on the top right side is vertical to the solid line. Short solid lines connect the observation points and the fitted positions. Middle lines connect the 0.4 ms and 1 ms fitted positions with the same $\theta_{1\parallel}$. The proper motion of the pulsar is 192.6 km/s, with an angle $\delta$ 4.59 degree west of north, is marked with an arrow from a star at the top of the figure.

| $\theta_{1\parallel}$(mas) | $f_D$(mHz) | $\sigma_{f_D}$(mHz) | $\tau$(ms) | $\sigma_\tau$(ms) | RA(mas) | $\sigma_{RA}$(mas) | dec(mas) | $\sigma_{dec}$(mas) | time(day) |
|---|---|---|---|---|---|---|---|---|---|
| -8.29 | -12.94 | 0.19 | 0.0845 | 0.0005 | 2.87 | 0.11 | -8.201 | 0.088 | 49.9 |
| -10.71 | -16.80 | 0.28 | 0.14123 | 0.0009 | 3.86 | 0.07 | -10.563 | 0.053 | 64.5 |
| -12.36 | -18.92 | 0.23 | 0.188 | 0.002 | 5.06 | 0.20 | -10.58 | 0.13 | 74.4 |
| -13.44 | -20.40 | 0.49 | 0.222 | 0.003 | 5.55 | 0.30 | -11.73 | 0.21 | 80.8 |
| -13.86 | -21.17 | 0.61 | 0.236 | 0.002 | 5.12 | 0.43 | -12.56 | 0.31 | 83.4 |
| -14.63 | -22.32 | 0.47 | 0.2633 | 0.0003 | 6.16 | 0.14 | -14.15 | 0.10 | 88.0 |
| -16.29 | -24.63 | 0.40 | 0.327 | 0.003 | 6.49 | 0.29 | -14.06 | 0.20 | 98.0 |
| -16.57 | -24.94 | 0.44 | 0.338 | 0.0003 | 8.29 | 0.42 | -14.37 | 0.32 | 99.7 |
| -17.44 | -26.09 | 0.36 | 0.3743 | 0.0006 | 8.53 | 0.52 | -15.74 | 0.42 | 105 |
| ··· | -35.06 | 0.52 | 0.950 | 0.002 | -15.23 | 0.69 | -21.06 | 0.70 | 202 |
| ··· | -38.31 | 0.64 | 0.9763 | 0.0009 | -15.02 | 0.48 | -20.74 | 0.38 | 190 |
| ··· | -40.17 | 0.55 | 1.0045 | 0.008 | -14.14 | 0.66 | -22.27 | 0.62 | 187 |
| ··· | -41.27 | 0.54 | 1.037 | 0.003 | -11.28 | 0.93 | -19.2 | 1.1 | 188 |
| ··· | -43.08 | 0.44 | 1.066 | 0.005 | -8.4 | 1.7 | -24.1 | 1.4 | 185 |

**Table 1.** 0.4 ms and 1 ms observation data and derived data. The upper part of the table list the 0.4 ms observation data. Observation data include the differential frequency $f_D$, time delay $\tau$ from scintillation measurement; RA and dec from the VLBI measurement. The method of how to calculate the error of time delay, differential frequency and the last column time is mentioned in Section 2.1. $\theta_{1\parallel}$, the angle of the 0.4 ms group with the component in the axis defined by $\alpha$, are derived from the $\theta - \tau$ relation plotted in Figure 1.

| Lens 1 $\theta_{1\parallel}$ (mas) | Lens 2 $\theta_{2\parallel}$(mas) | Observation $\tau$(ms) | $\sigma_\tau$(ms) | Calculated $\tau$(ms) | Observation $f_D$(mHz) | $\sigma_{f_D}$(mHz) | Calculated $f_D$(mHz) |
|---|---|---|---|---|---|---|---|
| -13.86 | -12.71 | 0.950 | 0.003 | 0.955 | -35.06 | 0.80 | -37.22 |
| -14.63 | -14.69 | 0.9763 | 0.0009 | 0.9763 | -38.31 | 0.79 | -38.31 |
| -16.29 | -15.78 | 1.005 | 0.008 | 1.0272 | -40.17 | 0.68 | -40.64 |
| -16.57 | -16.35 | 1.037 | 0.003 | 1.036 | -41.27 | 0.69 | -41.04 |
| -17.44 | -17.44 | 1.066 | 0.005 | 1.066 | -43.08 | 0.57 | -42.26 |

**Table 2.** Comparison of the observation time delay $\tau$ and the differential frequency $f_D$ of the observation data and the calculated result in double lens model. $\theta_{1\parallel}$ is the angle of the 0.4 ms group with the component in the axis defined by $\alpha$. $\theta_{2\parallel}$ is the angle of the 1 ms group with the component in the axis defined by $\alpha$.

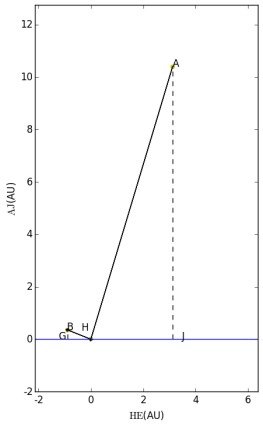


**Figure 3.** Refraction on lens 2. A is the position of the pulsar. H is the lensed image on lens 2. B is the lensed image on lens 1. J is the pedal of A to lens 2, and G is the pedal of B to lens 2. $v_{\rm JH}$ and $v_{\rm HG}$ should be equal, which is described in Section 2.4. In this case, $\theta_{1\parallel} = -17.44$ mas.

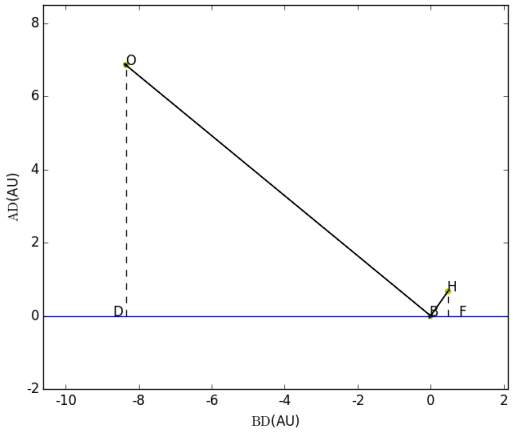


**Figure 4.** Refraction on lens 1. H is the lensed image on lens 2. B is the lensed image on lens 1. O is the position of the observer. F is the pedal of H to lens 2, and D is the pedal of O to lens 2. $v_{\rm FB}$ and $v_{\rm BD}$ should be equal, which is described in Section 2.4. In this case, $\theta_{\parallel} = -17.44$ mas.

Angular resolution can be improved using longer baselines, for example adding a GMRT-GBT baseline doubles the resolution. Observing at multiple frequencies over a longer period allows for a more precise measurement: when the pulsar is between two lenses, the refraction angle $\beta$ is small, and one expects to see the lensing at higher frequency, where the resolution is higher, and distances between lenses positions can be measured to much higher accuracy.

Holographic techniques (Walker et al. 2008; Pen et al. 2014) may be able to measure delays, fringe rates, and

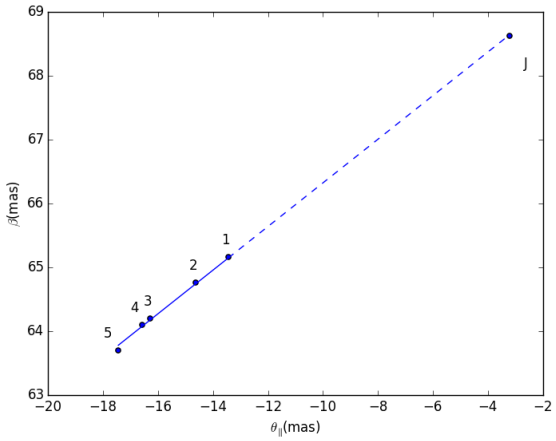


**Figure 5.** Incoming velocity in AJ direction minus refracted velocity in JA direction over the speed of light $\frac{v_{\rm AJ}-v_{\rm JA}}{c}$. $\beta_J$ is calculated with the first lensed image on lens 2 located at J, and $\theta_{1\parallel} = -3.21$ mas.

VLBI positions sbstantially more accurately. Combining these techniques, the interstellar lensing could conceivably achieve distance measurements an order of magnitude better than the current published effective distance errors. This could bring most pulsar timing array targets into the coherent timing regime, enabling arc minute localization of gravitational wave sources, lifting any potential source confusion.

Ultimately, the precision of the lensing results would be limited by the fidelity of the lensing model. In the inclined sheet model, the images move along fold caustics. The straightness of these caustics depends on the inclination angle, which in turn depends on the amplitude of the surface waves.

## 4 CONCLUSIONS

We have applied the Pen & Levin (2014) inclined sheet model to archival apex data of PSR B0834+06. The data is well fit by two linear lensing screens, with nearly plane-parallel geometry. This appears a natural consequence of very smooth reconnection sheets, and are an unlikely outcome of ISM turbulence. These results, if extrapolated to multi-epoch observations of binary systems, this might result in accurate distance determinations.

## 5 ACKNOWLEDGEMENTS

We thank NSERC for support.

## REFERENCES

Boyle L., Pen U.-L., 2012, Phys. Rev. D, 86, 124028
Brisken W. F., Macquart J.-P., Gao J. J., Rickett B. J., Coles W. A., Deller A. T., Tingay S. J., West C. J., 2010, ApJ, 708, 232
Pen U.-L., Levin Y., 2014, MNRAS, 442, 3338
Pen U.-L., Macquart J.-P., Deller A. T., Brisken W., 2014, MNRAS, 440, L36
Walker M. A., Koopmans L. V. E., Stinebring D. R., van Straten W., 2008, MNRAS, 388, 1214